Apoptosis (2009) 14:1165–1175
DOI 10.1007/s10495-009-0390-2

ORIGINAL PAPER

Comprehensive analysis of expression pattern and promoter regulation of human autophagy-related genes

Yusuke Kusama · Kazuyuki Sato · Naoko Kimura · Jun Mitamura · Hiroaki Ohdaira · Kenichi Yoshida

Published online: 6 August 2009

Abstract Autophagy is a highly conserved pathway for the degradation and recycling of long-lived proteins and cytoplasmic organelles. Similar to apoptosis, autophagy is a critical regulatory mechanism for determining cellular fate and various pathophysiological conditions in metazoans. So far, the systematic analysis of the expression patterns and transcriptional regulation of autophagy-related (ATG) genes has remained incompletely defined. In this study, we used RT-PCR to analyze the expression patterns of 26 human ATG genes simultaneously using cDNA derived from different adult and fetal tissues. As a result, we observed a characteristic ubiquitous expression pattern for all the genes except for ATG2A, ATG9B, and WIPI2. In particular, ATG2A was the only upregulated gene in the etoposide-induced apoptosis of HeLa cells. ATG2A mRNA was also upregulated by doxorubicin. Furthermore, we demonstrated that 13 out of 23 human ATG gene promoters were regulated by the transcription factor E2F1 in HeLa cells, indicating that these constructs could be useful for examining how the autophagy pathway is involved in other cellular phenomena, such as apoptosis evoked by various stimuli. Taken together, these results suggest that autophagy might be regulated at both the transcriptional level and the post-translational level.

Keywords Autophagy · Apoptosis · Human · Promoter · Expression

Introduction

Autophagy, which literally means "self-eating", is a unique and fundamental mechanism responsible for the degradation of cellular long-lived proteins and organelles that simultaneously recycles components to maintain cellular homeostasis; autophagy is often functionally related to apoptosis on a molecular level [1–5]. Autophagy is induced in response to nutrient starvation and has tissue-specific functions, though a basal level of autophagy is maintained as a housekeeping process in most cells [6, 7]. More than thirty autophagy-related (ATG) genes have been identified by yeast genetics, and recent advances in our understanding of the molecular mechanism underlying autophagy have enabled the spatiotemporal regulation of the formation of specific protein complexes during autophagy to be revealed. These protein complexes are mainly involved in three well-characterized processes: microautophagy, macroautophagy (generally referred to as autophagy), and chaperone-mediated autophagy [8–11]. In mammals, approximately two dozen homologs of the yeast ATG genes have been identified, strongly implying that these genes might also be involved in the pathogenesis of various diseases including cancer, neurodegenerative disease, and cardiac disease [12–14]. To date, whether autophagy promotes or hinders the progression of such diseases remains uncertain [15, 16].

To reveal the functional aspects of the human autophagy pathway, we focused on uncovering the mechanism responsible for the transcriptional regulation of the following human ATG genes: ULK1 and ULK2 (UNC51-like

Electronic supplementary material The online version of this article (doi:10.1007/s10495-009-0390-2) contains supplementary material, which is available to authorized users.

Y. Kusama · K. Sato · N. Kimura · J. Mitamura · H. Ohdaira · K. Yoshida (✉)
Department of Life Sciences, Faculty of Agriculture, Meiji University, 1-1-1 Higashimita, Tama-ku, Kawasaki, Kanagawa 214-8571, Japan
e-mail: yoshida@isc.meiji.ac.jp

kinases 1 and 2, respectively), ATG2A, ATG2B, ATG3, ATG4A (AUTOPHAGIN 2), ATG4B (AUTOPHAGIN 1), ATG4C, ATG4D, ATG5, BECN1 (BECLIN 1), ATG7, GABARAP (gamma-aminobutyric acid type-A receptor-associated protein), GABARAPL1 (APG8L), GABARAPL2 (GATE16), MAP1LC3A and MAP1LC3B (microtubule-associated protein 1, light chain 3, alpha and beta, respectively), ATG9A, ATG9B, ATG10, ATG12, ATG16L1, WIPI1 (WD40 repeat protein interacting with phosphoinositides 1), WIPI2, WIPI3 (WDR45L), WIPI4 (WDR45), and DRAM (damage-regulated autophagy modulator). Most of these numbered genes were named in accordance with their homologous counterparts found in model organisms, but exceptional gene names also exist. ULK1 and ULK2 have been identified as mammalian Atg1 homologs [17, 18]. BECN1 has been shown to be structurally similar to the yeast Vps30 (Atg6) gene [19]. GABARAP, GABARAPL1, GABARAPL2, and MAP1LC3 have been recognized as yeast Atg8 homologs [20]. And WIPIs are considered to be homologous to yeast Atg18 [21].

Among the above-mentioned ATG genes, the transcriptional regulations of ULK1, ATG5, MAP1LC3B, and DRAM are known to be governed by the transcription factor E2F1, and DRAM is also regulated by p53 [22, 23]. These findings suggest that transcriptional regulation might be involved in the link between autophagy and apoptosis, since E2F1 and p53 together play a pivotal role in the induction of apoptosis by orchestrating the expressions of their target genes [24]. In addition, the possible role of autophagy in cancer has been partly explained by the fact that DRAM is inactivated in certain cancers [25]. Moreover, human cells carrying mono-allelic deletions of the BECN1 gene and Becn1 heterozygous mice clearly showed a tendency toward tumorigenesis [19, 26, 27], indicating that subtle transcriptional deregulation might be a rate-limiting step in autophagy-involved human pathogenesis.

In the present study, we conducted a transcriptional analysis of human ATG genes by examining the distributions of their mRNA expressions during tissue development and etoposide-induced apoptosis. Our results clearly suggest that the majority of human ATG genes are ubiquitously expressed in adult and fetal tissues; however, a few genes are expressed in a tissue-specific manner. Interestingly, ATG2A was uniquely upregulated during the etoposide- and doxorubicin-induced apoptosis of HeLa cells, suggesting that ATG2A could be a novel biomarker of topoisomerase II inhibitor-mediated apoptosis. We also succeeded in establishing promoter-luciferase constructs of 23 human ATGs, and this set of constructs might be useful for examining how autophagy is involved in other cellular processes in human somatic cells, at least at the transcriptional level.

Materials and methods

Cell culture and chemicals

Human HeLa cervical adenocarcinoma cells were cultured in Earle's modified Eagle's medium (MEM) (Invitrogen, Carlsbad, CA) supplemented with 10% fetal bovine serum (FBS), 1% non-essential amino acids (Invitrogen), and antibiotic-antimycotics (Invitrogen) in a 5% CO_2 humidified atmosphere at 37°C. Etoposide and doxorubicin hydrochloride were purchased from Wako Pure Chemical Industries (Osaka, Japan). Chemicals were dissolved in dimethyl sulfoxide (DMSO) as 100 mM stock solutions and kept at −20°C until dilution before use. The final concentrations of etoposide and doxorubicin were 1×10^{-5} and 1×10^{-6} M, respectively.

In silico analysis

The expression profile was determined (May 29, 2009) based on the EST (expressed sequence tag) counts in human tissues and organs in the UniGene database (EST Profile Viewer, NCBI). The data sets used for the human ATG genes are listed in Supplementary Table 2. The number of transcripts per million (TPM) was calculated based on the gene EST/total EST in the pool, and this value was exported to an Excel file. Transcription factor binding motif was searched by TRANSFAC algorithm (threshold > 85) supported by GenomeNet (http://www.genome.jp/).

Reverse transcription-polymerase chain reaction (RT-PCR)

Total RNA was purified using an RNeasy mini kit (Qiagen, Valencia, CA) according to the manufacturer's instructions. Two micrograms of total RNA were reverse transcribed using High-Capacity cDNA Reverse Transcription kits (Applied Biosystems, Foster City, CA). The PCR was carried out in 25 µl of a mix consisting of 1× buffer, 200 µM dNTPs, 400 nM primers, 1 mM $MgSO_4$, 5% DMSO and 1 unit of KOD plus DNA polymerase (Toyobo, Osaka, Japan). Hot-start PCR was then performed as follows: denaturation for 3 min at 94°C followed by *ad libitum* cycles at 94°C for 15 s, a gene-specific annealing temperature (Table 1) for 30 s, and 68°C for 30 s, followed by an extension step of 2 min at 68°C. The PCR results were verified by varying the number of PCR cycles for each cDNA and set of primers. The target gene primer pairs were listed in Table 1. The amplified products were separated on 1.0 ~ 1.5% agarose gels and visualized under ultraviolet transillumination. The gel images were processed using Quantity One (Bio-Rad Laboratories, Hercules, CA). Briefly, each specific band was quantified

Table 1 Sequence of primers used for RT-PCR

Gene name	Sense primer sequence (5′–3′)	Antisense primer sequence (5′–3′)	Annealing temperature (°C)	PCR product length (bp)	GenBank accession number
ULK1	GTCCAGCTTTGACAGTCAGT	TCCCAGGACTCAGGATTCCA	52	480	NM_003565
ULK2	TGTTTCTAGGGTGTAGCTGG	CACCATCTACCCCAAGACCT	52	450	NM_014683
ATG2A	ACCTACACACGAGTGAGCGG	TGCCATGGTAATCCAGCCAG	63	420	NM_015104
ATG2B	GTGAGAGTCCTCTCTGGCGA	CGAGAATCCAAATCGTACCC	53	460	NM_018036
ATG3	CCAACATGGCAATGGGCTAC	ACCGCCAGCATCAGTTTTGG	58	420	NM_022488
ATG4A	GGAGGAGTTCATTGCTTCCC	GCATGGCCTGCAAAGCCCAA	54	500	NM_052936
ATG4B	TGCCTGTCCTGGGAAAGTAT	GGTCAAGGTGTCCCACACAT	52	390	NM_013325
ATG4C	TGCACATTGAGAACTGGCCA	ATGCCTTGCTTCTTCAACTG	55	420	NM_032852
ATG4D	CAGCCCACTGTGGATGTCAG	GCTCAAGATCCCACACCCGA	60	420	NM_032885
ATG5	AGTATCAGACACGATCATGG	TGCAAAGGCCTGACACTGGT	59	590	NM_004849
BECN1	ACTGTGTTGCTGCTCCATGC	CCCAAGCAAGACCCCACTTA	60	400	NM_003766
ATG7	CACTGTGAGTCGTCCAGGAC	CGCTCATGTCCCAGATCTCA	60	380	NM_006395
GABARAP	ACATTGCCTACAGTGACGAA	TTTCAGTCCCTTCCAACTAC	58	420	NM_007278
GABARAPL1	GTTGAGCATCCCTGTCTAAC	CTGACAGAACTGACACACAC	53	500	NM_031412
GABARAPL2	CGTGGAGTCCGCGAAGATTC	AGGCATGAGGACAATGCACA	63	530	NM_007285
MAP1LC3B	AAAGCTGTGGATGATCCACG	AGCAGGTGACAGGAACTCCT	52	480	NM_022818
ATG9A	ATGGGCAGTCGGCATCAAGG	CCCTGCTTGGCAGCTTCTAT	65	440	NM_001077198
ATG9B	CCACCTTGGGCAGTTCTTCT	CCTGCATGGTGAGAATGGTG	60	480	NM_173681
ATG10	CCAAGAGTTTACCTGGCCAG	CCTGGGTTAAAGCCAACCTC	59	380	NM_031482
ATG12	GAGACCAGCCTGGTTAGCAA	CTGAACCCTCAGTGGCAAAC	56	420	NM_004707
ATG16L1	AGAAGAAGCACATGGGCTCC	CAGGGAGGGGTCTGTAGTTC	60	460	NM_030803
WIPI1	CAGTAACACCGAGACGGTAC	GCACTTGGTCTGGCTACGGT	54	420	NM_017983
WIPI2	CGCACTGTAAGATGAGGCAG	ACTGGCGCAGCAGTAAGAGT	58	410	NM_015610
WIPI3	TGGCTGTGACCAGCTCGACT	GTGACGTCACGGGCACAGAT	60	420	NM_019613
WIPI4	TGACATAGCCTGTGTGTCTC	TCAAGGTACACGTCGAAAGC	59	480	NM_007075
DRAM	TGAGCCTGGGACTTCGAGAC	CTCAAGGAGCTCCCAATCTA	54	520	NM_018370

The annealing temperatures, PCR product lengths, and GenBank Accession numbers are also indicated

by volume analysis using the background subtraction method and the resulting density was represented as the ratio of etoposide/DMSO. The target gene bands were also compared to the corresponding GAPDH (glyceraldehyde-3-phosphate dehydrogenase; R&D Systems, Minneapolis, MN) band. For the cDNA panel analysis, 2.5 μl of cDNA purchased from Clontech (Mountain View, CA) was used (Human MTC panel I and II, Fetal MTC panel, and MCF7 apoptosis cDNA panel). The G3PDH primer in the kit was used as a control to amplify 983-bp.

Quantitative real-time RT-PCR

Real-time PCR was performed using a MiniOpticon machine (Bio-Rad Laboratories) with Power SYBR Green PCR Master Mix (Applied Biosystems). All the primers were tested to produce proportional changes in the threshold cycle with various initial quantities of cDNA. The measured threshold cycles (*Ct*) were converted to relative copy numbers using primer-specific standard curves. The *Ct* values were used to plot a standard curve in which *Ct* decreased in linear proportion to the log of the template copy number. The correlation values of the standard curves were always >90%. The gene expression levels induced by etoposide were normalized by the average levels of the mean-centered housekeeping gene GAPDH. All the samples were assayed in duplicate. All the values in the experiments were expressed as the mean ± SD (standard deviation) and were compared using two-tailed Student *t*-tests.

Promoter plasmids

Promoter fragments were generated using the PCR method from human genomic DNA (Promega, Madison, WI) and were ligated into the respective enzyme sites (Table 2) of the pGL3-Basic vector (Promega). The PCR primers are listed in Table 2. All the plasmid sequences were verified by sequencing at the Takara facility (Mie, Japan). Differences found by sequencing were compared with the

Table 2 Sequence of primers used for promoter-luciferase constructs

Gene name	Sense primer sequence (5′–3′)	Antisense primer sequence (5′–3′)	Flanking enzyme site	GenBank accession number	Amplified region (bp)
ULK1	TGTTCGTCACGCCCGGCTCT	GGATCCGACTCCGACTCCGA	KpnI/BglII	AC131009	−184 ~ 6
ULK2	GCCTGTCACCGTCCCTCTAG	CGACGTCCGCGCGCCTTGAA	KpnI/BglII	AC015726	−478 ~ −32
ATG2A	TCCTCTGGGGAAGGCTTCTA	CCATCGTGACATCTCGGAGA	KpnI/BglII	AC000159	−402 ~ 68
ATG2B	TCTTCTTCCTTCCTCCGGAG	CCCTATTTGGTGCCGGGAGT	KpnI/BglII	AL359240	−210 ~ 250
ATG3	CCAGCGTACTGTAGGAATAG	GCCACCGACTCGCATCAGCA	KpnI/BglII	AC092692	−866 ~ 24
ATG4A	TTCGCCGACGTCGCCGACTG	TGTGAGGGCAGCAAAGGCGC	KpnI/BglII	AL031177	−341 ~ 19
ATG4B	CACGTCCGTACCGCAAGATG	CCAATAGGTGTGCCGGCGCA	KpnI/BglII	AC133781	−261 ~ 19
ATG4C	CAGTTCCTACGCCAGAGGCA	CACACGCAGACGTTCCGACC	KpnI/BglII	AC103923	−345 ~ 45
ATG4D	TGCCCCGGAGGTCACACTAG	GCCATCGCCATCTTAGCGGG	KpnI/BglII	AC011461	−460 ~ −41
ATG5	AATGCCTGCGGTGGTTCCAA	TCCGTGTTCTGCCTAACCCA	KpnI/BglII	AL138917	−378 ~ −29
BECN1	AATAGCGGAGCCTCCCCATT	CTCTGTCTTCAGCGACTTCC	KpnI/BglII	AC055866	−207 ~ 13
ATG7	AGGTCCTGGGGGTAAGGAAA	GTAGCTGCCGCCATTATTTC	KpnI/HindIII	AC020750	−325 ~ 25
GABARAP	CCTACTTCGCGCACCCGCCA	GATCCACGAATTTGCGCCAC	KpnI/HindIII	AC120057	−653 ~ −1
GABARAPL1	GAGGCTGGATCCCAACCAGC	GGGAGCACAAAAACAGCTGG	KpnI/BglII	AC115676	−339 ~ 1
GABARAPL2	ATGAACCGCTCTAAGAGCCC	CGGCTGTCGGAGCCTAGCAA	KpnI/BglII	AC025287	−321 ~ 9
MAP1LC3A	TCGCCCTAAGCCCCGTGAAG	CCCGGTGACGTCAGGTCACA	KpnI/BglII	AL118520	−384 ~ 6
MAP1LC3B	ACTGCGCCCAGAATGAAGGC	ATGGGCGAAACGCGCGCTCT	KpnI/BglII	AC010531	−568 ~ −49
ATG9A	AACTGGCCCGCGTAAACTCG	ACTCACTGTCACCCGCAGCC	KpnI/BglII	AC068946	−303 ~ 7
ATG9B	ACACCTGGCTCTAACACGAT	GATGGGAGCTGTTGTTGCTT	KpnI/BglII	AC010973	−295 ~ 45
ATG10	CCTTTCACTTCTTCGCCTGC	GCCTCCTTCAGTCAGGTCCG	KpnI/BglII	AC114969	−673 ~ 17
ATG12	GCGAGAAGAACGAGTTCCAC	GGTCGAATGCGCACACTCCA	KpnI/BglII	AC022111	−745 ~ 5
ATG16L1	CCCTGTACCAAGCACAGTGC	CTACGCAGGGCGCTCGCTAG	KpnI/BglII	AC013726	−389 ~ 21
DRAM	GTGATGGCTATTCACGGCGC	AAGCGGACGCGACTACGGAG	KpnI/BglII	AC005409	−444 ~ 166

The amplified genomic region is indicted by numbering relative to the transcription initiation site (at +1) described in the NCBI UniGene Database (Genome View). The GenBank Accession numbers of the genomic clones were used to designate the PCR primers

deposited reference sequence in GenBank (Accession numbers are shown in Table 2). Differences in the following plasmid sequences were identified: ATG3 (G was changed to C at −221 position), ATG7 (T was changed to A at −199 position), GABARAPL1 (T was changed to C at −144 position), MAP1LC3B (A was changed to G at −474 position), ATG10 (T was deleted from T stretch at −479 position), and DRAM (G was changed to A at −417 position), where the minus position is relative to a transcriptional start site at +1.

Luciferase assay

For the promoter assay, 2×10^4 cells were transfected with FuGENE6 (Roche, Basel, Switzerland) according to the manufacturer's instructions. Briefly, 200 ng of the expression plasmid (pcDNA3 and pcDNA3-E2F1), 200 ng of the firefly luciferase reporter plasmids pGL3-Basic (Promega) or pTA-Luc, pE2F-TA-Luc (Clontech), and 0.6 ng of the *Renilla* luciferase reporter plasmid pRL-TK (Promega) per 24-well dish were used for each transfection. Cells were lysed 24 h after transfection by applying 100 μl of Passive Lysis Buffer of the Dual Luciferase Reporter Assay Kit (Promega) into each well of the 24-well plate. Five microliters of cell lysate were used for the luciferase reporter assay with the same kit, according to the manufacturer's protocol. Light intensity was quantified in a GloMax 20/20n Luminometer (Promega). The experiments were performed at least in triplicate. As a control for the transfection efficiency, the firefly luciferase activity values were normalized to the *Renilla* luciferase activity values. Data are presented as the mean value ± SD. Statistical differences were analyzed using two-tailed Student *t*-tests. A value of $P < 0.05$ was considered statistically significant.

Caspase-3/7 assay

The induction of apoptosis was assessed using a Caspase-Glo 3/7 assay according to the manufacturer's instructions (Promega). Briefly, the cells were inoculated into a 96-well plate at a concentration of 1×10^4 cells/well 24 h before treatment. The cells were then treated with chemicals for

48 h, followed by 1 h of incubation with Caspase-Glo 3/7 substrate at room temperature, and the resulting activity was measured using a GloMax 20/20n Luminometer (Promega). The activity was presented as relative light units (RLU, $\times 10^6$) in the treated cells relative to the control value (treated with 0.1% DMSO). Blanks were measured in wells containing 0.1% DMSO or chemicals without cells. The data are presented as the mean values ± SD. Statistical differences were analyzed using a two-tailed Student *t*-test. A value of $P < 0.05$ ($n = 3$) was considered statistically significant.

Results

Expression patterns of human ATG genes in adult and fetal tissues

Reports on the mRNA expression patterns of human ATG genes have been increasing in number; however, these reports have utilized different detection methods, such as Northern blot or RT-PCR, and different mRNA resources (summarized in Supplementary Table 1). Alternatively, EST counts for sequenced cDNA pools can be utilized as predictable information on the mRNA distribution patterns in various tissues and developmental stages for most of the human ATG genes (summarized in Supplementary Table 2); however, these data should be verified using a single detection method and a uniform cDNA resource. To achieve this goal, we performed RT-PCR for 23 human ATG genes in 16 adult tissues (heart, brain, placenta, lung, liver, skeletal muscle, kidney, pancreas, spleen, thymus, prostate, testis, ovary, small intestine, colon, and leukocyte) and 8 fetal tissues (brain, lung, liver, kidney, heart, spleen, thymus, and skeletal muscle) (Fig. 1). Most of the human ATG genes as well as G3PDH were ubiquitously expressed in the adult and fetal tissues that we examined, with a few exceptions (Fig. 1). Of note, the expression of ATG2A was not detected in adult tissues including the heart, brain, placenta, lung, liver, and skeletal muscle (Fig. 1). To our knowledge, the expression pattern of ATG2A has not been previously reported. ATG7 was expressed faintly in adult heart (Fig. 1), though the EST count both in literature and the UniGene database predicted that ATG7 would be expressed ubiquitously (Supplementary Tables 1 and 2) [28]. ATG9B showed a characteristic expression pattern in several RT-PCR analyses. Namely, ATG9B was abundantly expressed in some adult (placenta and testis) and fetal (brain, lung, and thymus) tissues, whereas none or a minimal expression level was observed in other adult (heart, lung, liver, skeletal muscle, kidney, pancreas, ovary, and colon) and fetal (liver, heart, and skeletal muscle) tissues (Fig. 1), though previously reported Northern blot and RT-PCR analyses predicted an ubiquitous pattern with the highest expression level thought to occur in the placenta (Supplementary Table 1) [29, 30]. The ATG9B expression pattern predicted by the EST count was tissue specific, with abundant expression in the placenta and ovary and medium or minimal expression in the lung, testis, liver, muscle, brain, and pancreas (Supplementary Table 2). These results support the notion that ATG9B mRNA exists in specific tissues and is most abundantly observed in the placenta. WIPI2 has been reported to exhibit a ubiquitous expression pattern, with the highest levels observed in the heart, skeletal muscle, and pancreas (Supplementary Table 1) [21]; however, our repeated RT-PCR experiments showed that WIPI2 was undetected in adult tissues including the heart, brain, placenta, lung, skeletal muscle, and kidney (Fig. 1). At present, we have no explanation for this discrepancy. DRAM expression was ubiquitous, with the highest level observed in the pancreas (Fig. 1), whereas the EST counts failed to show a high count in the pancreas and no counts were observed for the spleen (Supplementary Table 2). Together, these findings suggest that our comprehensive mRNA analysis of human ATG genes might be superior to EST counts and also to previous reports of individual experiments that were incomplete for most human ATG genes.

Changes in the expressions of human ATG genes in apoptotic cells

DRAM is a representative example of a gene that links autophagy and apoptosis, since DRAM is an essential factor for p53-mediated apoptosis and is also involved in autophagy [22]. Therefore, we checked the mRNA levels of human ATG genes regulated by apoptosis-inducing etoposide. HeLa cells were treated with 1×10^{-5} M of etoposide for 48 h, which was sufficient to induce caspases-3/7 activity (Fig. 2a). In addition, the accumulation of p53 protein accompanying an elevated phosphorylation level of serine 15 was detected 48 h after etoposide treatment, compared with the level in a DMSO vehicle treatment group (data not shown). Amongst the genes that were examined, the ATG2A and ATG4C mRNA levels were uniquely upregulated and downregulated, respectively, with a statistically significant difference (Fig. 2b, c). The expression level of DRAM was unchanged (Fig. 2b, c). We focused on ATG2A as an upregulated gene and further examined changes in the ATG2A transcript levels in HeLa cells using real-time PCR. Etoposide treatment increased the ATG2A mRNA level by 2.1-fold (SD = 0.0007, two-tailed Student *t*-test, $P = 0.02$, $n = 3$).

We reasoned that the upregulation of ATG2A mRNA might be a common phenomenon in apoptotic HeLa cells. Consequently, we treated the cells with doxorubicin;

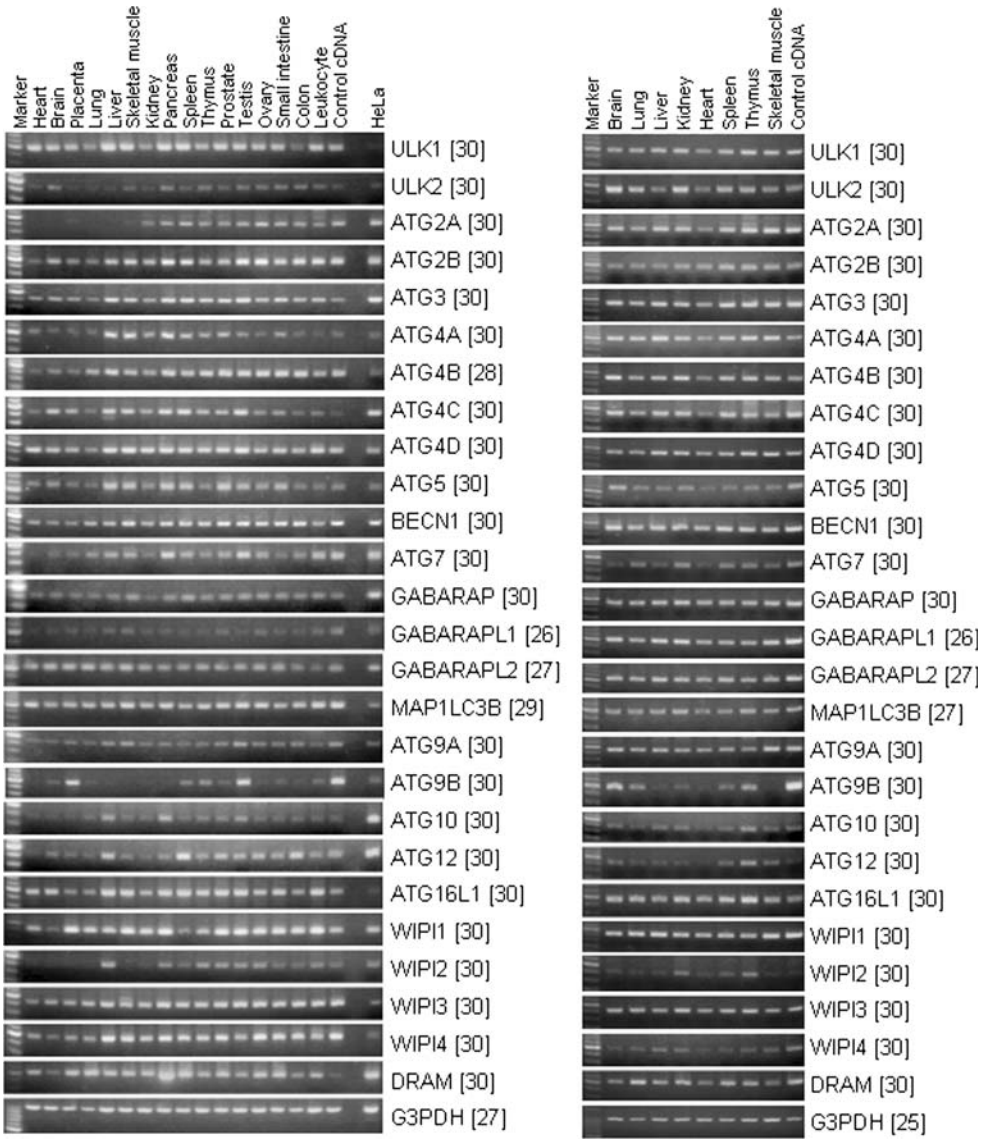

Fig. 1 Expression patterns of human ATG genes detected using RT-PCR. Multiple human adult (*Left panel*) and fetal (*Right panel*) tissues are indicated at the top. The *left panel* includes a cDNA derived from HeLa cells. Markers (100-bp ladder) are shown on the left side of the panel, with the 500-bp band highlighted. Gene names are shown on the right side of the panel. The value in *brackets* is the PCR cycling number. Note that different cycling numbers were used for ATG4B, MAP1LC3B, and G3PDH in the adult and fetal tissues

caspases-3/7 activity was clearly elevated in these cells, compared with DMSO-treated cells (Fig. 2d). The ATG2A mRNA level was upregulated in the doxorubicin-treated HeLa cells (Fig. 2e). In another cell line, MCF7, the ATG2A mRNA level was also upregulated by doxorubicin treatment in a time-dependent manner (Fig. 2f). In contrast, serum withdrawal for 48 h from HeLa cells failed to upregulate ATG2A mRNA level (Fig. 2g), suggesting ATG2A mRNA upregulation would be specific phenomenon of topoisomerase II inhibitor-mediated cell stress.

Regulation of promoter region of human ATG genes

Next, we focused on characterizing the promoter region of human ATG genes. For this purpose, we amplified and cloned the promoter regions of 23 human ATG genes into a pGL3-Basic luciferase reporter (Table 2). Recently, E2F1 has been reported to induce ATG1, MAP1LC3B, and DRAM directly and ATG5 indirectly [23]. Using a promoter reporter set, we checked whether the human ATG genes were responsive to E2F1 ectopic expression. Ectopic E2F1 expression in HeLa cells upregulated the luciferase activity of pE2F-TA-Luc (Fig. 3a). Surprisingly, a large number of promoter reporters, including those for ULK2, ATG4A, ATG4B, ATG4D, ATG7, GABARAPL2, MAP1LC3A, MAP1LC3B, ATG9A, ATG10, ATG12, and DRAM, were upregulated, based on the luciferase activity, whereas the promoter reporter of GABARAPL1 was downregulated (Fig. 3b). The ULK1 promoter region used in the luciferase assay was unchanged by E2F1 co-transfection, whereas a previous study utilizing the ULK1 promoter reported upregulation after E2F1 co-transfection [23]. This discrepancy might have been caused by the shorter ULK1 promoter region that was used in this study

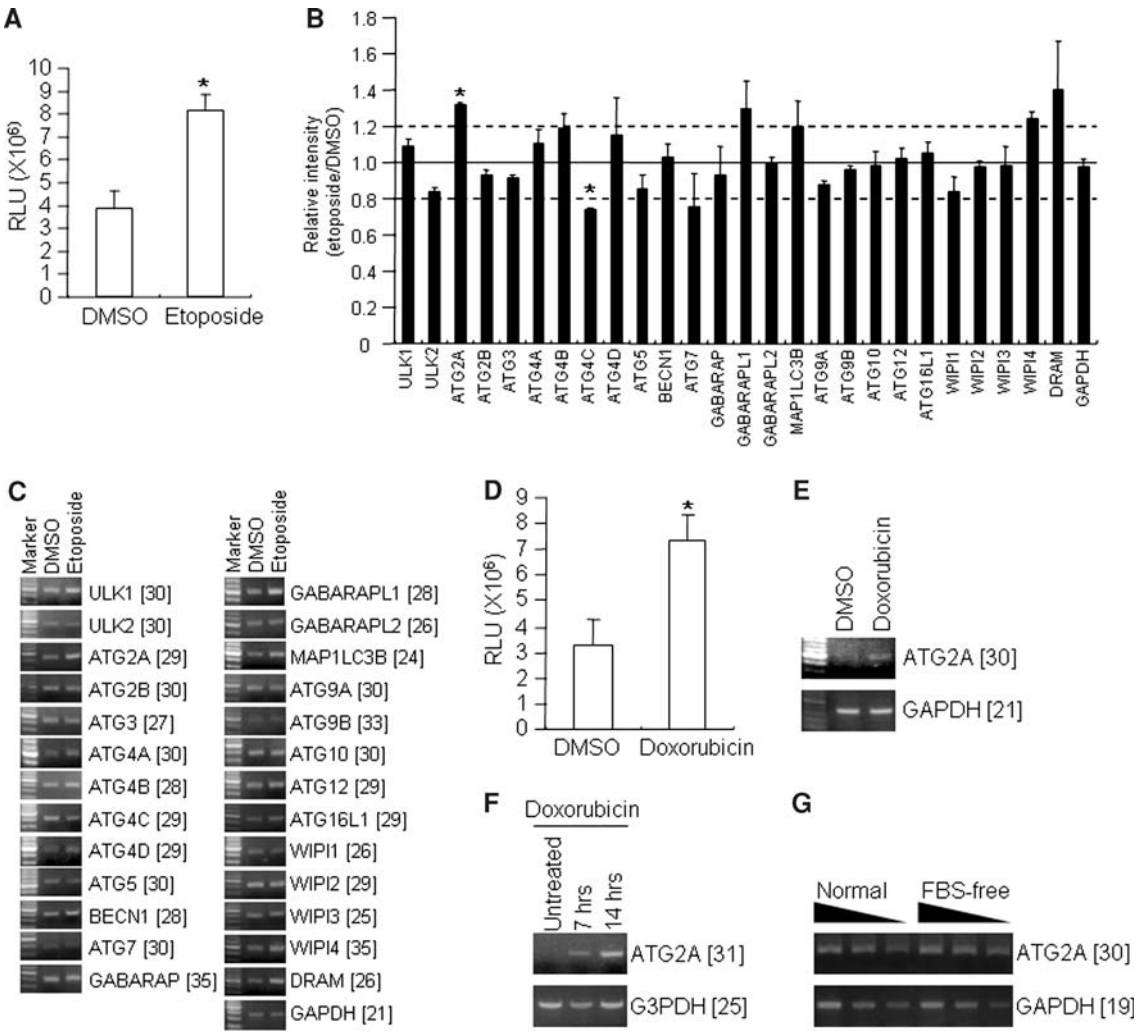

Fig. 2 Changes in the expressions of human ATG genes during apoptosis, as detected using RT-PCR. **a** Caspase-3/7 activity induced by etoposide. HeLa cells were treated with 1×10^{-5} M of etoposide for 48 h; the relative light units (RLU, $\times 10^6$) are expressed as the mean ± SD ($n = 3$). * $P < 0.05$ (compared with DMSO-treated cells), using a two-tailed Student *t*-test. **b** The mRNA levels induced by etoposide are shown as the relative intensity quantified by Quantity One software. The expression levels were divided by the DMSO-treated expression levels. Mean ± SD. * $P < 0.05$ compared with DMSO-treated control using a Student two-tailed *t*-test ($n = 2$). **c** Representative agarose gel images of RT-PCR results for etoposide-induced mRNA level changes. Markers (100-bp ladder) are shown on the left side of the panel, with the 500-bp band highlighted. Gene names are shown on the right side of the panel. The value in *brackets* is the PCR cycling number. **d** Caspase-3/7 activity induced by doxorubicin. HeLa cells were treated with 1×10^{-6} M of doxorubicin for 48 h; the relative light units (RLU, $\times 10^6$) are expressed as the mean ± SD ($n = 3$). * $P < 0.05$ (compared with DMSO-treated cells), using a two-tailed Student *t*-test. **e** ATG2A mRNA expression level in doxorubicin-treated or -untreated (DMSO) HeLa cells. GAPDH was detected as a control. The value in *brackets* is the PCR cycling number. **f** ATG2A mRNA expression level in doxorubicin-treated (7 and 14 h) or -untreated MCF7 cells. G3PDH was detected as a control. The value in *brackets* is the PCR cycling number. **g** ATG2A mRNA expression level in normal medium or serum withdrawal for 48 h from HeLa cells. *Filled rectangular triangle* indicates serial doubling dilution of cDNA template. GAPDH was detected as a control. The value in *brackets* is the PCR cycling number

(Fig. 3c), compared with that used in the previous study. Luciferase activity induced by ectopic E2F1 expression was not necessarily corresponding to the existence of predicted E2F consensus in the promoter region. In the presently reported promoter construct for DRAM, a p53 expression vector failed to induce luciferase activity (data not shown), suggesting that the p53-responsive sequences might be located outside of the −444 ∼166 region.

Discussion

In this study, we attempted to present a comprehensive picture of the transcriptional regulation of human ATG genes. First, we used uniform cDNA resources derived from various adult and fetal tissues for the PCR template and to verify whether human ATG genes are commonly or uniquely transcribed and to what extent, since a detailed

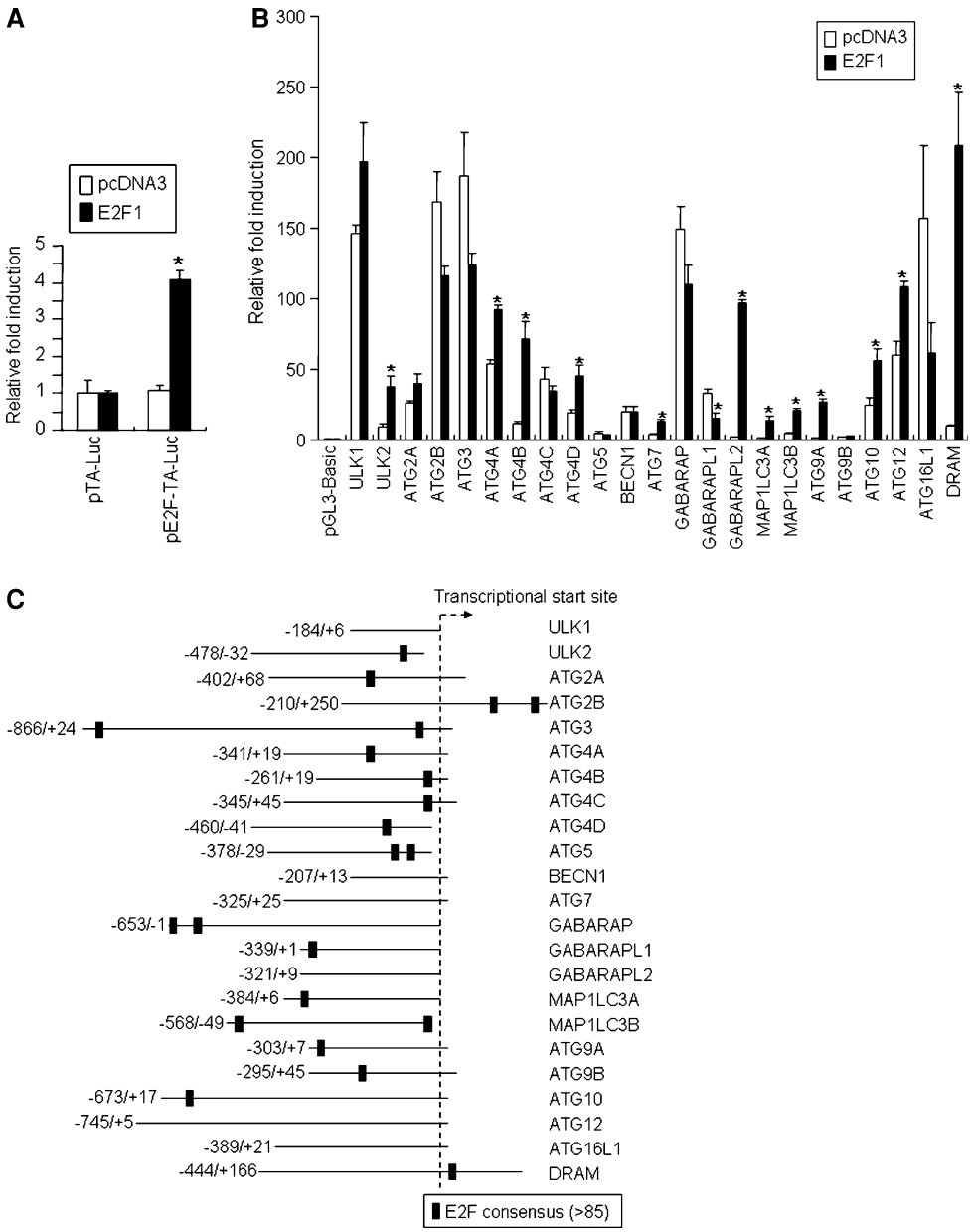

Fig. 3 Promoter-luciferase reporters of human ATG genes. HeLa cells were transfected with the indicated plasmids and luciferase activity was measured 24 h after transfection. For further details, please refer to the Materials & Methods section. **a** Induction level of reporter construct pE2F-TA-Luc bearing an E2F-binding sequence upstream of the luciferase gene in an E2F1 expression vector. The luciferase activity of pTA-Luc co-transfected with pcDNA3 (*white bar*) or pcDNA3-E2F1 (*black bar*) was set as 1, and the relative fold induction of pE2F-TA-Luc is shown. The values reported for the transfection experiments are the mean ± SD ($n = 3$, * $P < 0.05$). **b** Responsiveness of promoter region of human ATG genes to E2F1 expression. The luciferase activity of pGL3-Basic co-transfected with pcDNA3 (*white bar*) or pcDNA3-E2F1 (*black bar*) was set as 1, and the relative fold inductions of the indicated gene promoter constructs are shown. The values reported for the transfection experiments are the mean ± SD ($n = 3$, * $P < 0.05$). **c** The map of the promoter region of human ATG genes used for luciferase reporter constructs. The transcription start sites are indicated by the *bent arrows* and designated as "+1". *Positive* (*negative*) *numbers* are assigned to nucleotides downstream (upstream) of nucleotide +1. *Lines* with numbers are the regions used for the luciferase assay. The *black box* indicates the putative E2F binding site predicted by TRANAFAC (cut off score > 85)

examination of the mRNA distribution of human ATG genes has not been previously reported. Based on information available in medical literature, human ATG genes tend to be expressed ubiquitously [21, 28–39]. On the other hand, some exceptions exist. For example, ULK2 mRNA is abundant in ovary and testis, whereas little or no expression is present in the spleen [40]. ATG4B was highly expressed in skeletal muscle, but its expression was not detected in

fetal tissues [33]. MAP1LC3A expression was not detected in the thymus or peripheral blood leukocytes [38]. Our results suggest that ATG2A, ATG9B, and WIPI2 may be exceptional in that they exhibited specific mRNA expression patterns in certain adult tissues. ATG9B also showed a unique expression pattern in fetal tissues. Another characteristic feature of our analysis was that the mRNA expression levels of human ATG genes in the heart tended to be lower than that in other tissues. Autophagy is known to be maintained at a low basal level in the heart for the turnover of organelles under normal conditions and it is upregulated in response to stresses such as ischemia/reperfusion and in cardiovascular diseases such as heart failure [41].

The present results give an overall picture of the tissue distribution of ATG genes and therefore may provide a clue as to the establishment of conditional knockout mice. Observations using a mouse model suggest that autophagy plays critical roles in early or specific developmental processes [42]. For example, Atg5 null mice showed almost normal phenotypes at birth but died within 1 day of delivery as a result of energy depletion arising from reduced amino acid concentrations in plasma and tissues [43]. Further analysis of Atg5 null mice revealed that an increased number of apoptotic cells were observed in the retina and lung, partly because of a defect in dead cell clearance [44]. Neural-cell-specific Atg5 null mice showed progressive defects in motor function [45]. Additionally, Atg5 has been shown to be required for T and B lymphocyte survival during development [46, 47]. Unlike Atg5 null mice, Atg4C null mice were viable and fertile and did not display any obvious abnormalities [33], whereas Becn1 null mice died early during embryogenesis [27]. Atg7 deficiency in the central nervous system resulted in behavioral defects and resulted in death within 28 weeks of birth [48]. The conditional loss of Atg7 revealed that Atg7 is required for the starvation-induced degradation of proteins and organelles [49]. Mice carrying a beta cell-specific deficiency in Atg7 showed impaired glucose tolerance and a decreased serum insulin level [50]. Atg8 null mice died within 24 h after birth, similar to the Atg5 null mice [51]. An analysis of Atg16L1 deficient or hypomorphic mice demonstrated that Atg16L1 is responsible for controlling the endotoxin-induced inflammatory immune response and can serve as a model for Crohn's disease based on its characteristic role in the intestinal epithelium [52, 53].

The relation between autophagy and apoptosis can be explained by the fact that BCL-2, an anti-apoptotic protein, can function as an anti-autophagy protein via its inhibitory interaction with BECN1 [54]. In addition, ATG5 was originally identified as an upregulated protein during apoptosis [55]. Recently, *Drosophila* Atg1 overexpression has been shown to induce autophagy and apoptosis [56], indicating physiological levels of ATG genes are essential for autophagy, but unregulated levels of some ATG genes, such as ATG2A as well as *Drosophila* Atg1, would tend to be ended as inappropriate autophagy and apoptosis. Accumulated evidences imply that the spatiotemporal architecture of protein complex formation is crucial for determining the involvement of autophagy in other cellular machinery; however, transcriptional regulation must be a somewhat important regulatory step. For example, BNIP3, a hypoxia-inducible member of the BCL-2 family, is an essential regulator of hypoxia-induced autophagy and acts as a direct target of E2F1 [57]. Uniquely, E2F1 possesses dual roles in cell fate determination, such as cell cycle progression and apoptosis [24]. We demonstrated that 13 out of 23 human ATG gene promoters were regulated by E2F1, strongly indicating the mechanisms whereby autophagy pathway crosstalk with cell cycle regulation as well as apoptosis. We observed that ATG2A mRNA was specifically upregulated by etoposide in HeLa cells. The observed discrepancy between E2F1-regulated 13 promoters and etoposide-induced ATG2A mRNA can be explained by the fact that the etoposide-induced apoptosis is regulated not only by E2F1 but also by other multiple factors. A previous DNA microarray approach identified the upregulation of several ATG genes, including Atg2A, in dying salivary glands in *Drosophila* [58]. Basically, autophagy promotes cell survival, but in certain circumstances, autophagy contributes to cell death [59]. Together, these results suggest that the transcriptional regulation of ATG2A might be a unique indicator of autophagic programmed cell death, where apoptosis and autophagy are integrated to determine cell fate. To gain further insight into the role of ATG2A in autophagic cell death, functional assays should be performed in the future.

In summary, we have described the tissue distribution patterns of mRNAs for 26 human ATG genes. In addition, 23 promoter reporter constructs were produced in this study, and these constructs should serve as a unique tool for identifying signaling molecules that might be integrated into mTOR (mammalian target of rapamycin), a sensor kinase of growth factors and nutrient levels that regulates cellular growth and autophagy. Our present results imply that the transcriptional control of human ATG genes might partially contribute to human physiology and pathophysiology.

Acknowledgments This work was supported in part by Research Project Grant (B) by Institute of Science and Technology Meiji University. We thank Yuki Kumada, Kaori Hirano, Masahiro Kato, and Lin Cheming for technical support.

References

1. Baehrecke EH (2005) Autophagy: dual roles in life and death? Nat Rev Mol Cell Biol 6:505–510
2. Debnath J, Baehrecke EH, Kroemer G (2005) Does autophagy contribute to cell death? Autophagy 1:66–74

3. Yorimitsu T, Klionsky DJ (2005) Autophagy: molecular machinery for self-eating. Cell Death Differ Suppl 2:1542–1552
4. Klionsky DJ (2007) Autophagy: from phenomenology to molecular understanding in less than a decade. Nat Rev Mol Cell Biol 8:931–937
5. Maiuri MC, Zalckvar E, Kimchi A, Kroemer G (2007) Self-eating and self-killing: crosstalk between autophagy and apoptosis. Nat Rev Mol Cell Biol 8:741–752
6. Mizushima N, Klionsky DJ (2007) Protein turnover via autophagy: implications for metabolism. Annu Rev Nutr 27:19–40
7. Lum JJ, DeBerardinis RJ, Thompson CB (2005) Autophagy in metazoans: cell survival in the land of plenty. Nat Rev Mol Cell Biol 6:439–448
8. Klionsky DJ, Emr SD (2000) Autophagy as a regulated pathway of cellular degradation. Science 290:1717–1721
9. Kim J, Klionsky DJ (2000) Autophagy, cytoplasm-to-vacuole targeting pathway, and pexophagy in yeast and mammalian cells. Annu Rev Biochem 69:303–342
10. Mizushima N (2007) Autophagy: process and function. Genes Dev 21:2861–2873
11. Xie Z, Klionsky DJ (2007) Autophagosome formation: core machinery and adaptations. Nat Cell Biol 9:1102–1109
12. Yoshimori T, Noda T (2008) Toward unraveling membrane biogenesis in mammalian autophagy. Curr Opin Cell Biol 20:401–407
13. Levine B, Kroemer G (2008) Autophagy in the pathogenesis of disease. Cell 132:27–42
14. Todde V, Veenhuis M, van der Klei IJ (2009) Autophagy: principles and significance in health and disease. Biochim Biophys Acta 1792:3–13
15. Shintani T, Klionsky DJ (2004) Autophagy in health and disease: a double-edged sword. Science 306:990–995
16. Mizushima N, Levine B, Cuervo AM, Klionsky DJ (2008) Autophagy fights disease through cellular self-digestion. Nature 451:1069–1075
17. Yan J, Kuroyanagi H, Kuroiwa A, Matsuda Y, Tokumitsu H, Tomoda T, Shirasawa T, Muramatsu M (1998) Identification of mouse ULK1, a novel protein kinase structurally related to C. elegans UNC-51. Biochem Biophys Res Commun 246:222–227
18. Yan J, Kuroyanagi H, Tomemori T, Okazaki N, Asato K, Matsuda Y, Suzuki Y, Ohshima Y, Mitani S, Masuho Y, Shirasawa T, Muramatsu M (1999) Mouse ULK2, a novel member of the UNC-51-like protein kinases: unique features of functional domains. Oncogene 18:5850–5859
19. Liang XH, Jackson S, Seaman M, Brown K, Kempkes B, Hibshoosh H, Levine B (1999) Induction of autophagy and inhibition of tumorigenesis by beclin 1. Nature 402:672–676
20. Hemelaar J, Lelyveld VS, Kessler BM, Ploegh HL (2003) A single protease, Apg4B, is specific for the autophagy-related ubiquitin-like proteins GATE-16, MAP1-LC3, GABARAP, and Apg8L. J Biol Chem 278:51841–51850
21. Proikas-Cezanne T, Waddell S, Gaugel A, Frickey T, Lupas A, Nordheim A (2004) WIPI-1alpha (WIPI49), a member of the novel 7-bladed WIPI protein family, is aberrantly expressed in human cancer and is linked to starvation-induced autophagy. Oncogene 23:9314–9325
22. Crighton D, Wilkinson S, O'Prey J, Syed N, Smith P, Harrison PR, Gasco M, Garrone O, Crook T, Ryan KM (2006) DRAM, a p53-induced modulator of autophagy, is critical for apoptosis. Cell 126:121–134
23. Polager S, Ofir M, Ginsberg D (2008) E2F1 regulates autophagy and the transcription of autophagy genes. Oncogene 27:4860–4864
24. Rogoff HA, Kowalik TF (2004) Life, death and E2F: linking proliferation control and DNA damage signaling via E2F1. Cell Cycle 3:845–846
25. Crighton D, Wilkinson S, Ryan KM (2007) DRAM links autophagy to p53 and programmed cell death. Autophagy 3:72–74
26. Qu X, Yu J, Bhagat G, Furuya N, Hibshoosh H, Troxel A, Rosen J, Eskelinen EL, Mizushima N, Ohsumi Y, Cattoretti G, Levine B (2003) Promotion of tumorigenesis by heterozygous disruption of the beclin 1 autophagy gene. J Clin Invest 112:1809–1820
27. Yue Z, Jin S, Yang C, Levine AJ, Heintz N (2003) Beclin 1, an autophagy gene essential for early embryonic development, is a haploinsufficient tumor suppressor. Proc Natl Acad Sci USA 100:15077–15082
28. Yuan W, Stromhaug PE, Dunn WAJ (1999) Glucose-induced autophagy of peroxisomes in Pichia pastoris requires a unique E1-like protein. Mol Biol Cell 10:1353–1366
29. Robb GB, Carson AR, Tai SC, Fish JE, Singh S, Yamada T, Scherer SW, Nakabayashi K, Marsden PA (2004) Post-transcriptional regulation of endothelial nitric-oxide synthase by an overlapping antisense mRNA transcript. J Biol Chem 279:37982–37996
30. Yamada T, Carson AR, Caniggia I, Umebayashi K, Yoshimori T, Nakabayashi K, Scherer SW (2005) Endothelial nitric-oxide synthase antisense (NOS3AS) gene encodes an autophagy-related protein (APG9-like2) highly expressed in trophoblast. J Biol Chem 280:18283–18290
31. Kuroyanagi H, Yan J, Seki N, Yamanouchi Y, Suzuki Y, Takano T, Muramatsu M, Shirasawa T (1998) Human ULK1, a novel serine/threonine kinase related to UNC-51 kinase of Caenorhabditis elegans: cDNA cloning, expression, and chromosomal assignment. Genomics 51:76–85
32. Tanida I, Tanida-Miyake E, Komatsu M, Ueno T, Kominami E (2002) Human Apg3p/Aut1p homologue is an authentic E2 enzyme for multiple substrates, GATE-16, GABARAP, and MAP-LC3, and facilitates the conjugation of hApg12p to hApg5p. J Biol Chem 277:13739–13744
33. Marino G, Uria JA, Puente XS, Quesada V, Bordallo J, Lopez-Otín C (2003) Human autophagins, a family of cysteine proteinases potentially implicated in cell degradation by autophagy. J Biol Chem 278:3671–3678
34. Hammond EM, Brunet CL, Johnson GD, Parkhill J, Milner AE, Brady G, Gregory CD, Grand RJ (1998) Homology between a human apoptosis specific protein and the product of APG5, a gene involved in autophagy in yeast. FEBS Lett 425:391–395
35. Liang XH, Kleeman LK, Jiang HH, Gordon G, Goldman JE, Berry G, Herman B, Levine B (1998) Protection against fatal Sindbis virus encephalitis by beclin, a novel Bcl-2-interacting protein. J Virol 72:8586–8596
36. Wang H, Bedford FK, Brandon NJ, Moss SJ, Olsen RW (1999) GABA(A)-receptor-associated protein links GABA(A) receptors and the cytoskeleton. Nature 397:69–72
37. Xin Y, Yu L, Chen Z, Zheng L, Fu Q, Jiang J, Zhang P, Gong R, Zhao S (2001) Cloning, expression patterns, and chromosome localization of three human and two mouse homologues of GABA(A) receptor-associated protein. Genomics 74:408–413
38. He H, Dang Y, Dai F, Guo Z, Wu J, She X, Pei Y, Chen Y, Ling W, Wu C, Zhao S, Liu JO, Yu L (2003) Post-translational modifications of three members of the human MAP1LC3 family and detection of a novel type of modification for MAP1LC3B. J Biol Chem 278:29278–29287
39. Mizushima N, Sugita H, Yoshimori T, Ohsumi Y (1998) A new protein conjugation system in human. The counterpart of the yeast Apg12p conjugation system essential for autophagy. J Biol Chem 273:33889–33892
40. Ishikawa K, Nagase T, Suyama M, Miyajima N, Tanaka A, Kotani H, Nomura N, Ohara O (1998) Prediction of the coding sequences of unidentified human genes. X. The complete sequences of 100 new cDNA clones from brain which can code for large proteins in vitro. DNA Res 5:169–176

41. Nishida K, Kyoi S, Yamaguchi O, Sadoshima J, Otsu K (2009) The role of autophagy in the heart. Cell Death Differ 16:31–38
42. Cecconi F, Levine B (2008) The role of autophagy in mammalian development: cell makeover rather than cell death. Dev Cell 15:344–357
43. Kuma A, Hatano M, Matsui M, Yamamoto A, Nakaya H, Yoshimori T, Ohsumi Y, Tokuhisa T, Mizushima N (2004) The role of autophagy during the early neonatal starvation period. Nature 432:1032–1036
44. Qu X, Zou Z, Sun Q, Luby-Phelps K, Cheng P, Hogan RN, Gilpin C, Levine B (2007) Autophagy gene-dependent clearance of apoptotic cells during embryonic development. Cell 128:931–946
45. Hara T, Nakamura K, Matsui M, Yamamoto A, Nakahara Y, Suzuki-Migishima R, Yokoyama M, Mishima K, Saito I, Okano H, Mizushima N (2006) Suppression of basal autophagy in neural cells causes neurodegenerative disease in mice. Nature 441:885–889
46. Pua HH, Dzhagalov I, Chuck M, Mizushima N, He YW (2007) A critical role for the autophagy gene Atg5 in T cell survival and proliferation. J Exp Med 204:25–31
47. Miller BC, Zhao Z, Stephenson LM, Cadwell K, Pua HH, Lee HK, Mizushima NN, Iwasaki A, He YW, Swat W, Virgin HWIV (2008) The autophagy gene ATG5 plays an essential role in B lymphocyte development. Autophagy 4:309–314
48. Komatsu M, Waguri S, Chiba T, Murata S, Iwata J, Tanida I, Ueno T, Koike M, Uchiyama Y, Kominami E, Tanaka K (2006) Loss of autophagy in the central nervous system causes neurodegeneration in mice. Nature 441:880–884
49. Komatsu M, Waguri S, Ueno T, Iwata J, Murata S, Tanida I, Ezaki J, Mizushima N, Ohsumi Y, Uchiyama Y, Kominami E, Tanaka K, Chiba T (2005) Impairment of starvation-induced and constitutive autophagy in Atg7-deficient mice. J Cell Biol 169:425–434
50. Jung HS, Chung KW, Won Kim J, Kim J, Komatsu M, Tanaka K, Nguyen YH, Kang TM, Yoon KH, Kim JW, Jeong YT, Han MS, Lee MK, Kim KW, Shin J, Lee MS (2008) Loss of autophagy diminishes pancreatic beta cell mass and function with resultant hyperglycemia. Cell Metab 8:318–324
51. Sou YS, Waguri S, Iwata J, Ueno T, Fujimura T, Hara T, Sawada N, Yamada A, Mizushima N, Uchiyama Y, Kominami E, Tanaka K, Komatsu M (2008) The Atg8 conjugation system is indispensable for proper development of autophagic isolation membranes in mice. Mol Biol Cell 19:4762–4775
52. Saitoh T, Fujita N, Jang MH, Uematsu S, Yang BG, Satoh T, Omori H, Noda T, Yamamoto N, Komatsu M, Tanaka K, Kawai T, Tsujimura T, Takeuchi O, Yoshimori T, Akira S (2008) Loss of the autophagy protein Atg16L1 enhances endotoxin-induced IL-1beta production. Nature 456:264–268
53. Cadwell K, Liu JY, Brown SL, Miyoshi H, Loh J, Lennerz JK, Kishi C, Kc W, Carrero JA, Hunt S, Stone CD, Brunt EM, Xavier RJ, Sleckman BP, Li E, Mizushima N, Stappenbeck TS, Virgin HWIV (2008) A key role for autophagy and the autophagy gene Atg16l1 in mouse and human intestinal Paneth cells. Nature 456:259–263
54. Pattingre S, Tassa A, Qu X, Garuti R, Liang XH, Mizushima N, Packer M, Schneider MD, Levine B (2005) Bcl-2 antiapoptotic proteins inhibit Beclin 1-dependent autophagy. Cell 122:927–939
55. Grand RJ, Milner AE, Mustoe T, Johnson GD, Owen D, Grant ML, Gregory CD (1995) A novel protein expressed in mammalian cells undergoing apoptosis. Exp Cell Res 218:439–451
56. Scott RC, Juhasz G, Neufeld TP (2007) Direct induction of autophagy by Atg1 inhibits cell growth and induces apoptotic cell death. Curr Biol 17:1–11
57. Tracy K, Dibling BC, Spike BT, Knabb JR, Schumacker P, Macleod KF (2007) BNIP3 is an RB/E2F target gene required for hypoxia-induced autophagy. Mol Cell Biol 27:6229–6242
58. Lee CY, Clough EA, Yellon P, Teslovich TM, Stephan DA, Baehrecke EH (2003) Genome-wide analyses of steroid- and radiation-triggered programmed cell death in *Drosophila*. Curr Biol 13:350–357
59. Meléndez A, Neufeld TP (2008) The cell biology of autophagy in metazoans: a developing story. Development 135:2347–2360